Available online at www.sciencedirect.com
ScienceDirect
Acta Materialia 57 (2009) 2029–2039
Acta MATERIALIA
www.elsevier.com/locate/actamat

Mechanical properties of Al-based metal matrix composites reinforced with Zr-based glassy particles produced by powder metallurgy

S. Scudino [a,*], G. Liu [a,b], K.G. Prashanth [a,c,1], B. Bartusch [a], K.B. Surreddi [a], B.S. Murty [c], J. Eckert [a,d]

[a] IFW Dresden, Institut für Komplexe Materialien, Postfach 27 01 16, D-01171 Dresden, Germany
[b] State Key Laboratory for Mechanical Behavior of Materials and School of Materials Science and Engineering, Xi'an Jiaotong University, Xi'an 710049, China
[c] Department of Metallurgical and Materials Engineering, Indian Institute of Technology Madras, Chennai – 600036, India
[d] TU Dresden, Institut für Werkstoffwissenschaft, D-01062 Dresden, Germany

Received 15 October 2008; received in revised form 15 January 2009; accepted 15 January 2009
Available online 18 February 2009

Abstract

Al-based metal matrix composites consisting of pure Al reinforced with different amounts of mechanically alloyed $Zr_{57}Ti_8Nb_{2.5}Cu_{13.9}Ni_{11.1}Al_{7.5}$ glassy powder were produced by powder metallurgy, and their mechanical properties were investigated by room temperature compression tests. The samples were consolidated into highly dense bulk specimens at temperatures within the supercooled liquid region in order to take advantage of the viscous flow behavior of the glassy powder. Compression tests show that the addition of the glass reinforcement increases the strength of pure Al from 155 to 250 MPa, while retaining appreciable plastic deformation with a fracture strain ranging between 70% and 40%. The yield strength and the elastoplastic deformation of such composites containing a high volume fraction of glassy particles were accurately modeled using a shear lag model and a self-consistent effective medium approach. Finally, the fracture characteristics of the reinforcing particles were rationalized using a proposed fracture criterion.

Keywords: Powder consolidation; Metal matrix composites; Metallic glasses; Mechanical properties; Effective medium approximation

1. Introduction

Among the advanced engineering materials for aerospace and automotive applications, Al-based metal matrix composites (MMC) are of great interest owing to their remarkable mechanical properties, including low density, high elastic modulus and strength, and good fatigue and wear resistance [1–5]. The driving force behind the development of MMC is the possibility to tailor their properties to meet specific requirements, which renders this type of material unique in comparison with conventional unreinforced materials [1–5].

MMC can be classified into three main groups: (i) fiber-reinforced, (ii) whisker/short-fiber/platelet-reinforced and (iii) particulate-reinforced composites [6]. Although the largest improvement in properties (strength and stiffness) is obtained with the introduction of fiber reinforcements [1,6], the properties of fiber-reinforced composites are not isotropic. Particulate-reinforced MMC show the advantage of nearly isotropic properties [1]. Furthermore, an additional advantage of the particulate-reinforced over fiber-reinforced MMC is that most existing processing techniques can be used for fabrication and finishing of

* Corresponding author. Tel.: +49 351 4659 838; fax: +49 351 4659452.
E-mail address: s.scudino@ifw-dresden.de (S. Scudino).
[1] Present address: Helmholtz Center Berlin for Materials and Energy, SF-3 (Structural Research), D-14109 Berlin, Germany.

1359-6454/$36.00 © 2009 Acta Materialia Inc. Published by Elsevier Ltd. All rights reserved.
doi:10.1016/j.actamat.2009.01.010

the composites, including hot rolling, hot forging, hot extrusion and machining [5,7].

Typical reinforcements in particulate-reinforced MMC are ceramics, such as Al_2O_3 and SiC [2,8,9]. However, more recently, metallic glasses have also been successfully used as reinforcement in Al-based MMC [10–12]. Metallic glasses are extremely attractive as reinforcing agents because of their remarkable mechanical properties, including high yield strength (1–2 GPa) and large elastic strain (1–2%) [13–16]. In addition, they may yield an improved interface between matrix and particles with respect to the more conventional ceramic reinforcements [10].

Powder metallurgy (P/M) is one of the methods successfully used for the preparation of MMC [2,4,8,17]. The main advantage of P/M over other methods, such as ingot metallurgy and diffusion welding, is the relatively low processing temperature, which may avoid undesired interfacial reactions between matrix and reinforcement [18]. In addition, P/M allows a great degree of freedom in tailoring the microstructure (e.g., volume fraction, size and morphology of the reinforcement) [2,4,8,10–12,17].

In this work, MMC consisting of pure Al reinforced with Zr-based glassy particles were produced by P/M, and their mechanical properties were investigated in detail. The glassy powders were obtained by mechanical alloying (MA) of elemental powders with composition $Zr_{57}Ti_8Nb_{2.5}Cu_{13.9}Ni_{11.1}Al_{7.5}$ (at.%), and the crystallization behavior as well as the temperature dependence of the viscosity of the glassy powders were studied in order to select the proper consolidation parameters. The glass-reinforced Al-based MMC were then consolidated through uniaxial hot pressing followed by hot extrusion, and the mechanical properties of the bulk specimens were evaluated by room temperature compression tests. Subsequently, a model description for the elastoplastic deformation of the composites, which is an important prerequisite for the material design and application, is given, revealing that the mechanical properties can be successfully modeled taking particle cracking into account. Finally, the distensile fracture of the present glassy particles is explained using calculation results and a suitable fracture criterion.

2. Experimental

Glassy powders with composition $Zr_{57}Ti_8Nb_{2.5}Cu_{13.9}Ni_{11.1}Al_{7.5}$ (purity > 99.9 wt.%) were produced by MA of pure elemental powder mixtures using a Retsch PM400 planetary ball mill and hardened steel balls and vials. The sample handling was carried out in a glove box under a purified argon atmosphere (<1 ppm O_2 and H_2O). The powders were milled for 120 h at a ball-to-powder mass ratio of 13:1, using a milling speed of 150 rpm. The amount of iron and oxygen after milling for 120 h was found to be ~0.10 and 0.30 wt.%. The viscosity of the samples as a function of temperature was measured by parallel plate rheometry in a Perkin-Elmer TMA7 thermal mechanical analyzer (heating rate 20 K min^{-1}). The phases and the microstructure were characterized by X-ray diffraction (XRD) using a Philips PW 1050 diffractometer (Co K_α radiation) and by scanning electron microscopy (SEM) using a Hitachi TM-1000 tabletop microscope. Al-based metal matrix composites consisting of elemental Al powder blended with different amounts (40 and 60 vol.%) of $Zr_{57}Ti_8Nb_{2.5}Cu_{13.9}Ni_{11.1}Al_{7.5}$ glassy powders were synthesized by P/M methods. Consolidation was done by uniaxial hot pressing followed by hot extrusion under an argon atmosphere at 673 K and 500 MPa. The extrusion ratio was 6:1. The density of the consolidated samples was evaluated by the Archimedes principle. According to the ASTM standard for compression testing [19], cylinders with a length/diameter ratio of 2.0 (8 mm length and 4 mm diameter) were prepared from the extruded samples. The specimens were tested with an INSTRON 8562 testing facility under quasistatic loading (strain rate 8×10^{-4} s^{-1}) at room temperature. Both ends of the specimens were polished to make them parallel to each other prior to the compression test.

3. Results and discussion

3.1. Sample characterization

The characterization of the $Zr_{57}Ti_8Nb_{2.5}Cu_{13.9}Ni_{11.1}Al_{7.5}$ glassy powder prepared by MA of elemental powder mixtures has been previously reported [20,21]. However, some key features should be quoted here. The as-milled powder is amorphous, and its crystallization behavior is characterized by an endothermic effect related to the occurrence of the glass transition (T_g) at 668 K, followed by the supercooled liquid (SCL) region ($\Delta T_x = T_{x1} - T_g$), limited by two exothermic crystallization events with onset temperatures T_{x1} (716 K) and T_{x2} (757 K). The first exothermic peak is related to the formation of an unidentified nanocrystalline phase [20,21], while the second peak is due to the formation of the tetragonal $CuZr_2$ phase (space group $I4/mmm$) and a minor amount of fcc $NiTi_2$-type big cube phase (space group Fd3m) [20,21].

In the temperature range between the glass transition (T_g) and the first crystallization event (T_{x1}) the glassy material may exhibit a deformation regime characterized by viscous flow behavior [22]. In this region, the viscosity of metallic glasses may decrease by several orders of magnitude, allowing the production of bulk samples by consolidation at temperatures within the range of the SCL region [22]. In order to verify this aspect and to select the proper consolidation temperature, the flow behavior of the $Zr_{57}Ti_8Nb_{2.5}Cu_{13.9}Ni_{11.1}Al_{7.5}$ glassy powder within the SCL was analyzed from viscosity measurements using parallel plate rheometry, and the results are shown in Fig. 1a. The viscosity η can be derived from the change in the height of the sample vs time as [23–25]

$$\eta = \left(\frac{2Fh^3}{3\pi a^4(dh/dt)}\right) \quad (1)$$

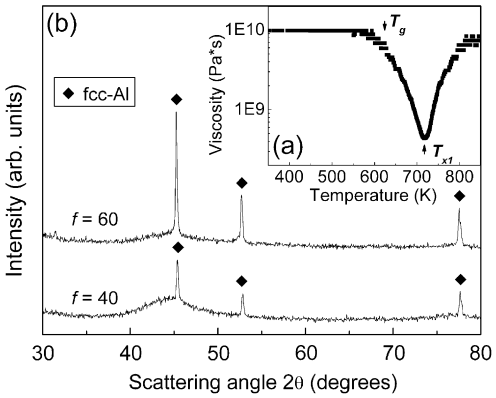

Fig. 1. (a) Temperature dependence of the viscosity (heating rate 20 K min^{-1}), revealing a drop in viscosity at T_g followed by an abrupt increase at T_{x1} due to crystallization. (b) XRD patterns (Co K_α radiation) for the hot pressed and hot extruded composites with 40 and 60 vol.% glass reinforcement.

where F is the applied load, a is the radius of the plates, and h is the height of the sample. This allows viscosity measurements in the range from 10^5 to 10^{10} Pa s [23,24]. The viscosity of the powder shows a constant value of $\sim 1\times10^{10}$ Pa s up to ~600 K, where the curve displays a strong drop in viscosity due to the occurrence of the glass transition. At ~717 K, where the glassy powder shows minimum viscosity, crystallization sets in, and the viscosity abruptly increases with increasing temperature, indicating the loss of the liquid-like behavior. These results indicate that the temperature range from 600 to 700 K, where softening of the material occurs, is suitable for the consolidation of the glass-reinforced composites.

3.2. Consolidation and mechanical properties

In order to produce glass-reinforced MMC, elemental Al powder was blended with different volume fractions (f) of $Zr_{57}Ti_8Nb_{2.5}Cu_{13.9}Ni_{11.1}Al_{7.5}$ glassy powder. The composite powders were then consolidated by hot pressing, followed by hot extrusion at 673 K in order to take advantage of the SCL regime. This gives rise to consolidated composites with a relative density ~98%. For comparison purposes, a bulk specimen was produced by extrusion of pure Al powder using the same consolidation parameters as used for the MMC.

Fig. 1b shows the XRD patterns of the composites reinforced with 40 and 60 vol.% of $Zr_{57}Ti_8Nb_{2.5}Cu_{13.9}Ni_{11.1}Al_{7.5}$ glassy powder ($f = 40$ and $f = 60$). The patterns display sharp Bragg peaks belonging to pure Al, together with the broad maxima due to the glassy phase. This indicates that no crystallization of the glass occurred during consolidation of the composites.

Fig. 2a and b shows the SEM micrographs of the composites with 40 and 60 vol.% glass reinforcement, respectively. The images display a microstructure consisting of approximately spherical bright particles (the glassy phase) with dimensions ~50 μm homogeneously dispersed in the

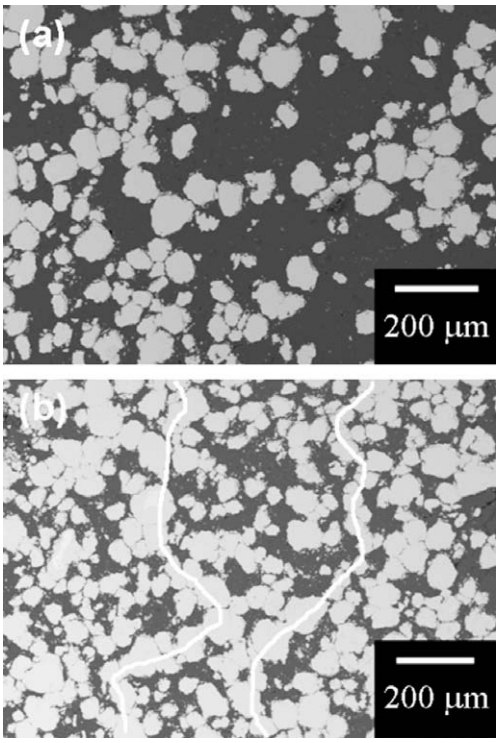

Fig. 2. SEM micrographs for the consolidated composites with (a) 40 vol.% and (b) 60 vol.% $Zr_{57}Ti_8Nb_{2.5}Cu_{13.9}Ni_{11.1}Al_{7.5}$ glass reinforcement.

fcc Al matrix. Owing to the high volume fractions of reinforcement, several particles are in contact. This gives rise to the formation of small groups of particles with dimensions ~100–200 μm. This effect increases with increasing volume fraction of reinforcement from 40 to 60 vol.%. Only a few pores are visible, further corroborating the high density of the consolidated specimens.

Typical room temperature uniaxial compression true stress–true strain curves of the tests under quasistatic loading for the composite materials are shown in Fig. 3 together

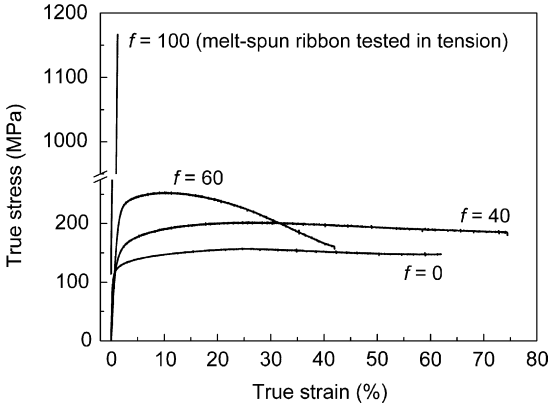

Fig. 3. Room temperature compression true stress–true strain curves for the hot pressed and hot extruded pure Al ($f = 0$), composites with 40 vol.% ($f = 40$) and 60 vol.% ($f = 60$) glass reinforcement, and melt-spun $Zr_{57}Ti_8Nb_{2.5}Cu_{13.9}Ni_{11.1}Al_{7.5}$ glassy ribbon tested in tension ($f = 100$).

with the curve for the extruded pure Al. In order to compare the data of the composites with those of the single-phase glass, the tensile stress–strain curve of the $Zr_{57}Ti_8Nb_{2.5}Cu_{13.9}Ni_{11.1}Al_{7.5}$ glassy ribbon produced by melt spinning is also plotted in Fig. 3. The mechanical properties of pure Al are improved by the addition of the glass reinforcement. The compressive strength (the maximum compressive stress which the material is capable of sustaining [26]) increases from 155 MPa for pure Al to 200 MPa for the composite with $f = 40$, while retaining a strain at the compressive strength exceeding 30% and a fracture strain ~70%. With the volume fraction of the glassy powder increasing to 60 vol.%, the compressive strength rises to ~250 MPa, and the strain at the compressive strength is ~10%. Both pure Al and the material with $f = 40$ show a weak work softening-like behavior for large strains. However, for the composite reinforced with 60 vol.% of glassy powder, the stress, after reaching the maximum value, displays a pronounced work softening-like behavior where the stress gradually decreases with increasing strain to 160 MPa, and fracture occurs at ~42% strain. Although the compressive strength of the composites is remarkably lower with respect to the single-phase glass (1150 MPa), the composite materials display fairly large plastic deformation which, in contrast, is absent for the single-phase glass.

As a typical example, Fig. 4 shows SEM micrographs of the fracture morphology for the composite with $f = 60$. The images reveal that, after deformation, several cracks appear in the reinforcing particles (Fig. 4a). Particle fracture occurs parallel to the compression direction (indicated by arrows in Fig. 4a). In contrast, the Al matrix undergoes large plastic deformation and displays dimple rupture, indicative of ductile fracture (Fig. 4b and c).

3.3. Modeling of mechanical properties

The prediction of the overall mechanical properties of a composite from the properties of the single constituents is an important prerequisite for material design and application. Among the different methods for estimating the properties of a composite, the rule of mixtures (ROM) is the simplest and most intuitive [27]. The ROM considers the properties of the composite as volume-weighted averages of the components' properties and assumes that the components are non-interacting during deformation [28,29]. This can be written as

$$P_c = f_m \cdot P_m + f_p \cdot P_p \quad (2)$$

where P is the property (e.g., density or yield strength), f is the volume fraction, and the subscripts c, m and p indicate the composite, the matrix and the reinforcement, respectively.

The ROM describes well the effect of the volume fraction of the reinforcement on the density of the composites, as shown in Fig. 5; however, it fails in modeling the strength of the materials. The experimental yield strength

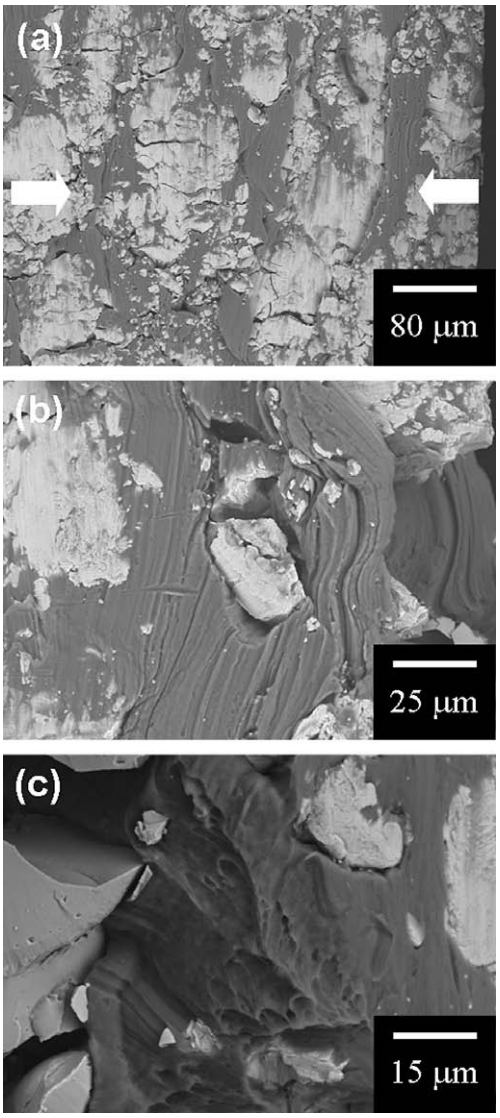

Fig. 4. SEM micrographs of the fracture morphology after compression test for the composite with 60 vol.% ($f = 60$) glass reinforcement.

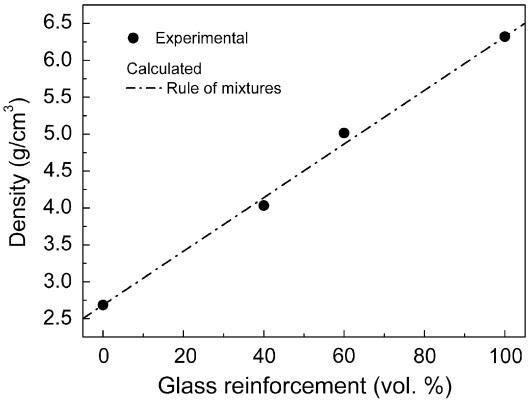

Fig. 5. Density of the samples as a function of the volume fraction of glass reinforcement (the sample with 100 vol.% corresponds to the $Zr_{57}Ti_8Nb_{2.5}Cu_{13.9}Ni_{11.1}Al_{7.5}$ rod produced by copper mold casting).

(offset = 0.2%) of the composites is much less than that predicted from the ROM (Fig. 6a).

As well as through the ROM, the strengthening effect of second-phase particles on the yield strength (σ_y) of the metallic matrix can be written as [30]

$$\sigma_y = \sigma_y^o + \sqrt{(\Delta\sigma_{or})^2 + (\Delta\sigma_{the})^2 + (\Delta\sigma_{geo})^2} \quad (3)$$

where σ_y^o is the strength of the pure metal matrix (equivalent to 113 MPa for the present extruded material), $\Delta\sigma_{or}$ is the Orowan stress or the stress increase needed to pass a dislocation through an array of impeding particles, $\Delta\sigma_{the}$ is the stress contribution due to statistically stored dislocations introduced by the thermal expansion mismatch between the matrix and second-phase particles, and $\Delta\sigma_{geo}$ is the stress contribution due to strain gradient effects associated with the geometrically necessary distributions of dislocations required to accommodate the plastic deformation mismatch between the matrix and the particles.

The Orowan stress can be written as [31]

$$\Delta\sigma_{or} = \varphi\frac{\mu^m b^m}{L} \quad (4)$$

where ϕ is a constant of order 2 [31], b^m and μ^m are the Burgers vector and the shear modulus of the metal matrix, respectively, and L is the interparticle spacing of the second phase particles, which is given by [31]

$$L = D\left(\frac{\pi}{6f}\right)^{1/3} \quad (5)$$

where f and D are the volume fraction and the diameter of the particles, respectively.

The stress increment due to thermal expansion mismatch is [32]

$$\Delta\sigma_{the} = \eta\mu^m b^m\sqrt{\rho} \quad (6)$$

where η is a constant of order 1, and ρ is the dislocation density. ρ is given by [33,34]

$$\rho = \frac{12\Delta T\Delta\alpha f}{b^m D(1-f)} \quad (7)$$

where $\Delta\alpha$ is the difference in thermal expansion coefficients (TEC) between the matrix and the reinforcing particles, and ΔT is the temperature change from processing temperature to room temperature.

Finally, the stress increment due to geometrically necessary dislocations is [35]

$$\Delta\sigma_{geo} = \beta\mu^m\sqrt{f\varepsilon^m b^m/D} \quad (8)$$

where β is a geometric factor with a numerical value ~0.4, and ε^m is the plastic strain of the metal matrix [35].

The yield strength of the current MMC reinforced with glassy particles was calculated using Eq. 3, and the parameters used in the calculation are summarized in Table. 1. The results reveal that Eq. 3 underestimates

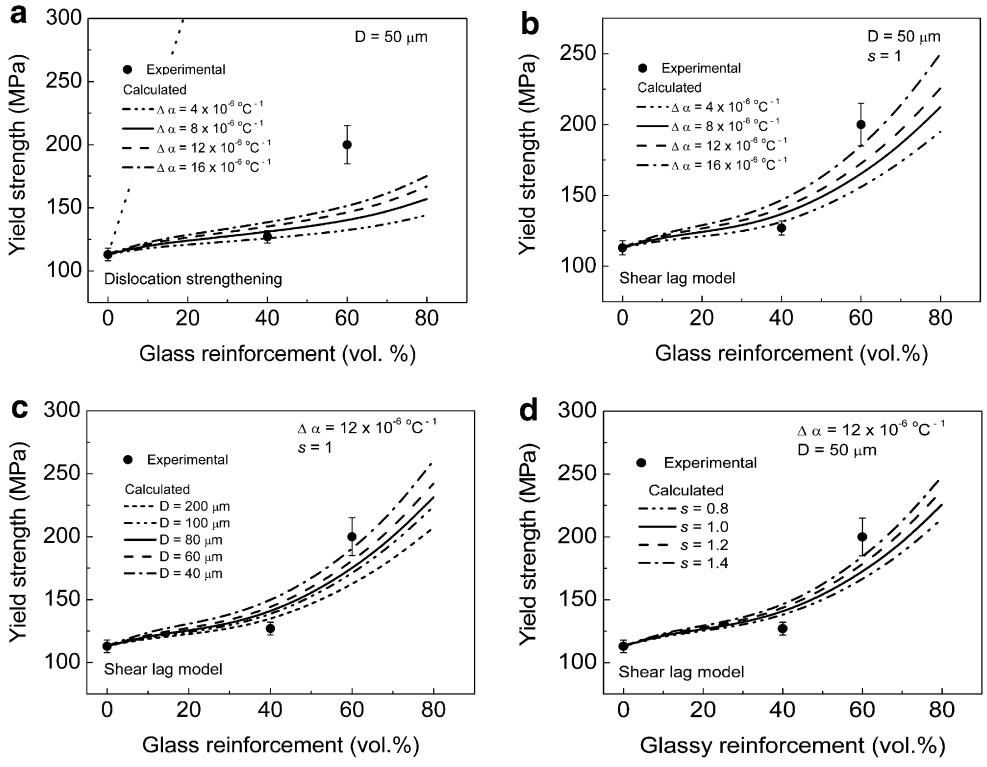

Fig. 6. Yield strength of the consolidated samples as a function of the volume fraction of glass reinforcement: experimental data (points) and calculated values (lines) from (a) dislocation strengthening, (b) shear lag model varying the difference in TECs $\Delta\alpha$, (c) shear lag model varying the particle size D and (d) shear lag model varying the particle aspect ratio s.

Table 1
Parameters used in calculations.

Parameter, unit	Value	Ref.
E^m, GPa	70	[36]
μ^m, GPa	28	[36]
ν^m	0.33	[36]
b^m, nm	0.283	[36]
E^p , GPa	100	[37]
μ^p, GPa	37	[37]
M	4.2	Calibrated

the experimental value of the yield strength for the sample with $f = 60$, as shown in Fig. 6a, which indicates that the strength increase in the present composites cannot be accurately explained by considering exclusively dislocation strengthening. This is most likely due to the high volume fraction and the relatively large size of the reinforcing particles and the resulting load transfer by shear. For volume fractions >50 vol.%, local particle contiguity can arise [38], and the percolation threshold can be exceeded. As a result, the number of particles in contact is higher than in the case of more dilute particles. Consequently, the particles may form a continuous network (represented by the white lines in Fig. 2b) and, during deformation, the connected particles will behave similarly to short fibers. The strengthening effect of the stress transfer can be taken into account using the shear lag model [39] for the evaluation of the yield strength for the sample with $f = 60$, as

$$\frac{\sigma_y^m}{\sigma_y} = f\left(\frac{E^p}{E^m} - \frac{E^p - E^m}{E^m}\frac{\tanh(\gamma s)}{\gamma s}\right) + (1 - f) \tag{9}$$

where E^m and E^p are the elastic moduli of matrix metal and particles, respectively, and s is the aspect ratio (l_p/l_v) of the reinforcing particles, where l_p and l_v are the particle size parallel to and vertical to the compressive testing direction, respectively. The particle size is then given by $D = \sqrt{l_p l_v}$. γ is a function of the elastic modulus of the matrix, the volume fraction of reinforcing particles and Poisson's ratio of the matrix (ν_m):

$$\gamma = \sqrt{\frac{2E^m}{E^p(1+\nu_m)\ln(1/f)}} \tag{10}$$

After these modifications, the calculations are in better agreement with the experimental results, as shown in Fig. 6b.

The second-phase particles used in the present work have an average size $D \approx 50$ μm. At this particle size, the contribution of $\Delta\sigma_{the}$ to the total yield strength is much larger than both $\Delta\sigma_{or}$ and $\Delta\sigma_{geo}$. As revealed in Eqs. 6 and 7, $\Delta\sigma_{the}$ depends on $\Delta\alpha$, D and f . In order to analyze the effect of TEC, particle size, particle contact and morphology, Fig. 6b–d shows the dependence of the yield strength on $\Delta\alpha$, D and aspect ratio s as functions of the volume fraction f. The calculations indicate that the influence of $\Delta\alpha$ on the yield strength of the composites is the most significant, even when particles of ~100–200 μm (the groups of particles visible in Fig. 2a) or the aspect ratios observed for the present particles ($s = 0.8$–1.4) are considered. The TEC of Al is $\sim 24 \times 10^{-6}$ °C^{-1} [1], and the TEC of Zr-based metallic glass is 10×10^{-6} °C^{-1} [40]. Therefore, the values of $\Delta\alpha$ used in the present calculations are reasonable.

Metal matrix composites reinforced with high-strength particles have been extensively studied in recent years owing to their attractive mechanical properties. However, few data exist on the mechanical properties of MMC containing high volume fractions ($f > 50$) of reinforcing particles [38,41]. Two main aspects make the deformation behavior of composites with high particle content different from that characterizing composites with small volume fractions of reinforcement. The first aspect is related to the local particle contiguity and the possible formation of a continuous particle network, as already discussed in the previous section. The second aspect involves the constraints for the deformation of the matrix introduced by the presence of a large number of particles. The metallic matrix is confined within a large number of particles and, therefore, cannot easily deform in response to the applied stress.

Effective medium approximation (EMA) based methods have been used successfully to model the elastoplastic deformation of metal matrix composites reinforced with micrometer-sized second-phase particles [42–46]. In the following, the EMA method will be used to evaluate the overall compressive mechanical behavior of the glass-reinforced MMC.

In this method, the particulate-reinforced composite is assumed to behave as a continuum. The constitutive relation between the average stress ($\bar{\sigma}$) and strain ($\bar{\varepsilon}$) in the composites can be written in terms of their secant stiffness C^* as

$$\bar{\sigma} = C^*(\bar{\varepsilon})\bar{\varepsilon} \tag{11}$$

For simplicity, the second-phase particles are considered as spherical particles, because the aspect ratio of the glassy particles used in present experiments is close to 1. In addition, the effect of the aspect ratio on the yield strength is limited (Fig. 6d). Two methods can be used to perform the EMA analysis [47]. The first method is the classical EMA in which the reference state is the metal matrix alone, namely $K^0 = K^m$ and $\mu^0 = \mu^m$, where K^0 (K^m) and μ^0 (μ^m) are the secant bulk and shear moduli of the effective reference medium (the matrix). The second method is the self-consistent EMA (SCEMA) in which the reference state corresponds to the composite material (matrix and reinforcement), and the values are obtained self-consistently, i.e., $K^0 = K^*$ and $\mu^0 = \mu^*$, where K^* and μ^* are the secant bulk modulus and the shear modulus of the composite, respectively. The former method is generally valid when the volume fraction of particles is small (typically <15 vol.%) while the latter is used for larger volume fractions of particles, therefore considering the elastic interactions between

the particles. In the present composites, the volume fraction of the glassy particles is high (40 and 60 vol.%), and some degree of connectivity between the particles is also observed. This implies that the interactions between the glassy particles have to be considered when modeling the deformation behavior of the composites and, therefore, the SCEMA method is used here. According to SCEMA, the effective moduli are given by the following expressions [47,48]

$$(1-f)\frac{K^m-K^*}{3K^m+4\mu^*}+f\frac{K^p-K^*}{3K^p+4\mu^*}=0 \tag{12-1}$$

$$(1-f)\frac{\mu^m-\mu^*}{\mu^m+y^*}+f\frac{\mu^p-\mu^*}{\mu^p+y^*}=0 \tag{12-2}$$

with

$$y^*=\frac{\mu^*(9K^*+8\mu^*)}{6(K^*+2\mu^*)} \tag{13}$$

where K^m and μ^m are the secant bulk and shear moduli of the matrix, and K^p and μ^p are the elastic and shear moduli of the particles. The hydrostatic (σ^m_{kk} and ε^m_{kk}) and the deviatoric (σ'^m_{ij} and ε'^m_{ij}) parts of the stress and the strain in the strengthened matrix can be related to those of the composites by

$$\varepsilon^m_{kk}=\frac{3K^*+4\mu^*}{3K^m+4\mu^*}\bar{\varepsilon}_{kk},\qquad \sigma^m_{kk}=\frac{3K^*+4\mu^*}{3K^m+4\mu^*}\frac{K^m}{K^*}\bar{\sigma}_{kk} \tag{14-1}$$

$$\varepsilon'^m_{ij}=\frac{\mu^*+y^*}{\mu^m+y^*}\bar{\varepsilon}'_{ij},\qquad \sigma'^m_{ij}=\frac{\mu^*+y^*}{\mu^m+y^*}\frac{\mu^m}{\mu^*}\bar{\sigma}'_{ij} \tag{14-2}$$

The stresses on the particles are

$$\sigma^p_{kk}=\frac{3K^m+4\mu^m}{3K^p+4\mu^m}\frac{K^p}{K^m}\sigma^m_{kk} \tag{15-1}$$

$$\sigma'^p_{ij}=\frac{\mu^m+y^*}{\mu^p+y^*}\frac{\mu^p}{\mu^m}\sigma'^m_{ij} \tag{15-2}$$

The uniaxial stress–strain behavior of the strengthened aluminum matrix can be expressed by the Ramburg–Osgood equation [1]

$$\varepsilon^m=\frac{\sigma^m}{E^m}+\alpha\frac{\sigma^m_y}{E^m}\left(\frac{\sigma^m}{\sigma^m_y}\right)^{1/n} \tag{16}$$

where E^m is Young's modulus for aluminum, n is the strain hardening exponent, and α is a dimensionless constant ($\alpha=3/7$ is usually taken for Al-based alloys [48]). σ^m_y is the optimized yield strength of the matrix obtained by Eq. 9 through the shear lag model. The secant Young's modulus of the isotropic matrix under uniaxial deformation is given by

$$E^{sm}=\frac{E^m}{1+\alpha\left(\frac{\sigma^m_{11}}{\sigma^m_y}\right)^{n/1-n}} \tag{17}$$

Based on the assumption of the plastic incompressibility for the matrix metal, the secant bulk modulus of the composites is equal to its linear elastic bulk modulus. The secant shear modulus is then given as

$$\mu^{sm}=\frac{E^{sm}}{3-E^{sm}/3K^m} \tag{18}$$

An iterative scheme is adopted to calculate the stress–strain ($\bar{\sigma}-\bar{\varepsilon}$) curves of the MMC. An initial value for σ^m_{11} is selected, from which the values of E^{sm} and μ^{sm} are obtained from Eqs. (17) and (18). These values are then used in Eq. (12) to calculate K^* and μ^*. Using these starting values, $\bar{\sigma}$ and $\bar{\varepsilon}$ can be obtained from Eq. (14). Increasing the value of σ^m_{11} and repeating the same process, $\bar{\sigma}-\bar{\varepsilon}$ curves can be obtained. The Considère criterion ($d\bar{\sigma}/d\bar{\varepsilon}<\bar{\sigma}$) is used to determine the moment of mechanical instability.

Based on the above model and using the parameters listed in Table 1, the stress–strain curves for the composites containing different volume fractions of particles can be calculated, as shown in Fig. 7a, and compared with the experimental results. The calculations are in good agreement with the experimental results only for the sample with $f=0$, the pure Al matrix. In contrast, the calculations strongly overestimate the deformation behavior of the samples with $f=40$ and $f=60$. This is most likely due to particle cracking during deformation, as observed in Fig. 4. When particle cracking and void formation increase to some degree, the composites can become mechanically instable, even at a low strain. The SCEMA method can take into account this additional aspect and can optimize the deformation behavior considering particle cracking.

Under the stress σ^p (Eq. (15)), the percentage of fractured particles (P^c_f) and the critical fracture stress of the particles (σ^p_{cra}) can be expressed by [49,50]

$$P^p_f=1-\exp\left[-\frac{f_c}{f_0}\left(\frac{\sigma^p}{\sigma^p_{cra}}\right)^m\right] \tag{19-1}$$

$$\sigma^p_{cra}=K_p/\sqrt{r} \tag{19-2}$$

where K_p is a constant calibrated from modeling that is related to the fracture toughness of the particles, r is the average particle radius, f_0 is the reference volume fraction that will crack at a probability of 63.2% under stress equal to σ^p_{cra}, and m is the Weibull modulus. The stresses on the particles increase with deformation (Eq. (15)). Therefore, particle cracking or void formation depends on the degree of deformation, which can be calculated from Eqs. (15) and (19).

Fig. 8a shows the predicted dependence of P^c_f on K_p as a function of stress and strain for the composite with 40 vol.% of glassy particles. The values of K_p used for the SCEMA calculations (2.0–2.8 MPa $m^{1/2}$) are close to that determined for ceramic particles in Al-based composites (2.4–2.8 MPa $m^{1/2}$) [46] and for intermetallic particles in Al-based alloys (1.3–2.0 MPa $m^{1/2}$) [47]. P^c_f gradually increases with increasing strain. The percentage of fractured particles P^c_f as a function of strain decreases with increasing K_p. In contrast, P^c_f slightly increases with increasing stress up to ~120 MPa, where the composite with 40 vol.% of reinforcement begins to yield, and then it sharply increases, reaching a value of P^c_f of ~20% at 170 MPa. In addition, P^c_f is significantly affected by the

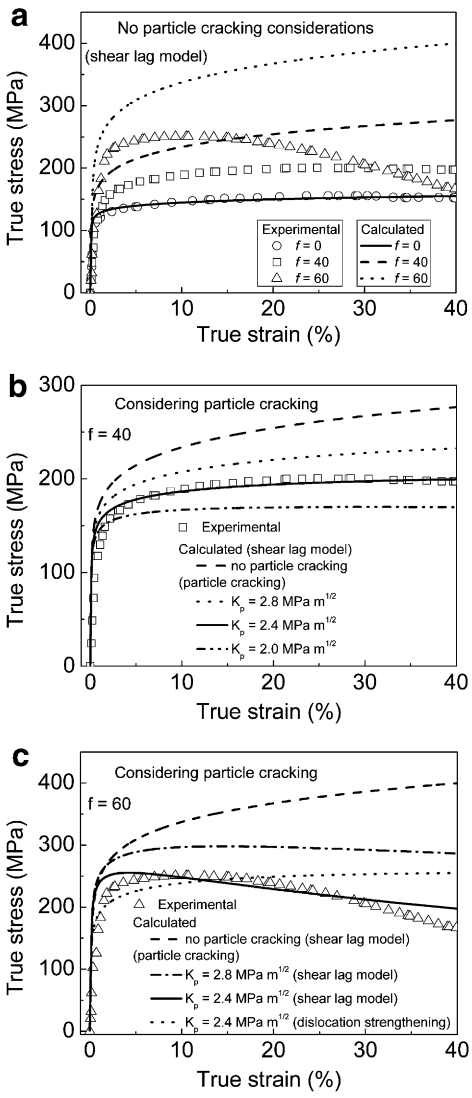

Fig. 7. (a) Room temperature compression stress–strain curves for the consolidated samples: experimental data (points) and values calculated by the shear lag model without any particle cracking considerations (lines). (b) Stress–strain curves for the composite with 40 vol.% ($f = 40$) glass reinforcement: experimental data (points) and values calculated by the shear lag model with and without considering particle cracking (lines). (c) Stress–strain curves for the composite with 60 vol.% ($f = 60$) glass reinforcement: experimental data (points) and values calculated by the shear lag model with and without considering particle cracking (lines). The stress–strain curve calculated by dislocation strengthening is also added for comparison.

particle size, as shown in Fig. 8b. The percentage of fractured particles vs strain increases with increasing particle size, indicating that large particles are prone to fracture at lower strains compared with smaller particles. As soon as the crack forms, a void is created, and the particle is no longer able to bear the applied load. As a result, the deformation behavior of the composites is sensitive to particle cracking, as observed in Fig. 7b and c.

The SCEMA model considering particle cracking accurately predicts the deformation behavior of both the composites with 40 and 60 vol.% of glass reinforcement when $K_p = 2.4$ MPa m$^{1/2}$ and the yield strength σ_y^m evaluated by the shear lag model are used in the calculations. For comparison, SCEMA calculations based on σ_y^m evaluated by dislocation strengthening only are also presented in Fig. 7c, further indicating that particle connectivity as well as particle cracking have to be taken into account to describe properly the mechanical behavior of the current glass-reinforced composites.

3.4. Fracture mechanism of the glassy particles

The fracture morphology of the deformed samples (Fig. 4a) reveals that, after compression, the glassy particles are fractured along the compressive direction, as schematically illustrated in Fig. 9a. This local fracture mode, defined as distensile fracture [51], is significantly different from the macroscopic fracture usually observed in bulk metallic glasses tested in compression, where the failure mode is shear fracture with a fracture plane close to 45° [52]. There have been some reports on a similar distensile fracture mode in compressed BMG composites containing ceramic particles, strong fibers or ductile dendrites [51–54]. In these BMG composites, the macroscopic distensile fracture results from the inhomogeneous stress distribution that is caused by the introduction of second phases [51]. In the present experiments, distensile fracture occurs locally within the fully glassy particles; however, it can be described taking into account the possible effects on the fracture mechanism as follows.

The stress state in a particle embedded in a deformed matrix is very complicated. However, the task can be simplified by analyzing the particle only and by assuming that the matrix merely serves to transfer the remote applied stress to the particle. In this way, the fracture of a glassy particle can be analyzed as in the case of monolithic bulk metallic glasses (BMG). Recently, a unified fracture criterion has been proposed to explain the fracture behavior of BMG [51,55]. This fracture criterion unifies the four classic fracture criteria, i.e., maximum normal stress criterion, Tresca criterion, Mohr–Coulomb criterion and von Mises criterion, and it has been applied successfully to explain the fracture behavior of different types of bulk metallic glasses [55]. The unified fracture criterion can lead to each of the four classic criteria when specific conditions are met. For example, when the critical normal fracture stress of the BMG is much less than the critical shear fracture stress, the new fracture criterion can be reduced to the classic maximum normal stress criterion [51]. The unified fracture criterion is used to analyze the distensile fracture of the glassy particle in the present composites.

Fig. 9b schematically illustrates the failure conditions of the metallic glass under tension and compression, where circles A and B are compressive and tensile Mohr circles. σ_c and σ_t are the intrinsic compressive and tensile fracture strength of the BMG, respectively, σ_0 is the intrinsic cleavage strength of the material under the condition without shear stress τ_n, and τ_0 is the intrinsic shear strength of the

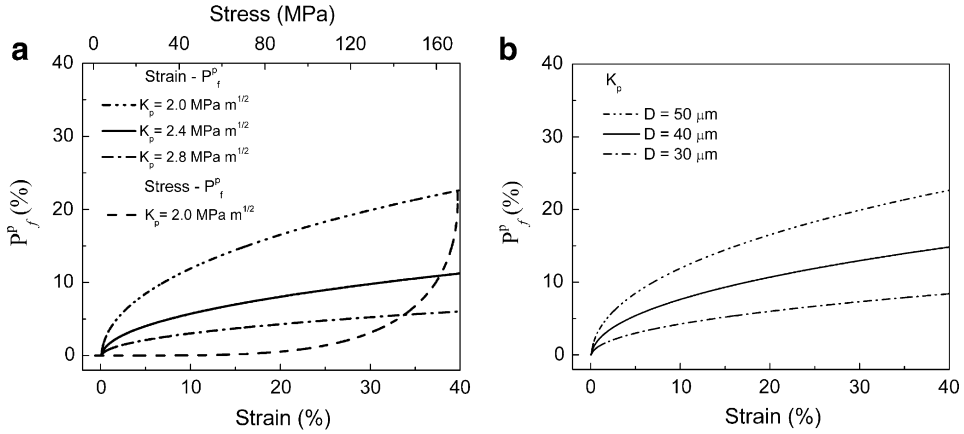

Fig. 8. (a) Predicted stress and strain dependence of the percentage of fractured particles P_f^c for different values of the fracture toughness of the particles K_p and (b) predicted strain dependence of P_f^c for different values of the particle size D for the composite with 40 vol.% glassy particles. Note that the stress values in (a) do not correspond to the strain values therein.

material under the condition without normal stress σ_n. At the right-hand side of Fig. 9b (tension condition), an ellipse criterion was recently developed to describe the fracture behavior as [55]

$$(\sigma_n/\sigma_0)^2 + (\tau_n/\tau_0)^2 = 1 \tag{20}$$

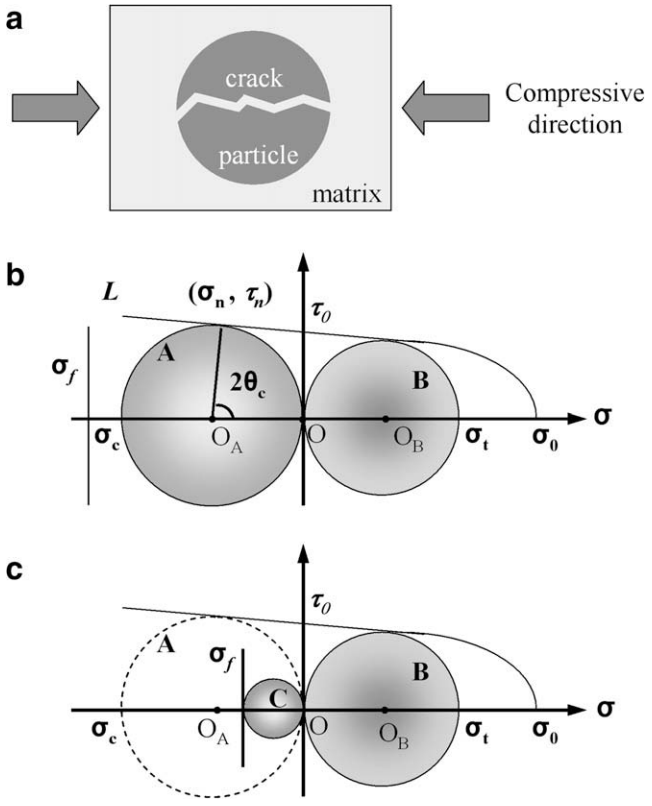

Fig. 9. (a) Schematic illustration of the fracture of the glassy particles during compression test. (b and c) Schematic illustrations of the fracture criterion for the evaluation of the fracture mode at different conditions: (b) $\sigma_f > \sigma_c$; (c) $\sigma_f < \sigma_c$.

At the left-hand side of Fig. 9b (compressive condition), the compressive Mohr circle will first touch the critical fracture line $\tau_0 L$ at the contact point (σ_n,τ_n) if the critical distensile fracture stress σ_f is $>\sigma_c$. At this condition, the fracture angle θ is

$$\theta = arctg(\sqrt{1+\Lambda^2} - \Lambda) \tag{21}$$

where Λ is the slope of the line $\tau_0 L$. From Eq. 21 it follows that θ, although somewhat smaller than 45°, is much larger than 0°. However, in the present experiments the distensile fracture of the glassy particles is characterized by $\theta \sim 0°$ (Figs. 4a and 9a). This implies that the value of σ_f for the present glassy particles is $<\sigma_c$. As shown in Fig. 9c, when $\sigma_f < \sigma_c$, the Mohr circle C will first touch the distensile fracture line σ_f rather than the critical fracture line $\tau_0 L$. As a result, the glassy particles will fracture in the direction almost parallel to the compressive axis, as observed in the present work. The strength of the $Zr_{57}Ti_8Nb_{2.5}Cu_{13.9}Ni_{11.1}Al_{7.5}$ glass is ~1150 MPa (Fig. 3), while the critical distensile fracture stress σ_f, evaluated in the previous section, is only ~480 MPa (i.e., $\sigma_f = \sigma^p_{cra} = 2.4/\sqrt{r}$, $r \approx 25 \times 10^{-6}$ m). The smaller value of σ_f with respect to σ_c can thus reasonably explain why the glassy particles fracture in a break or split mode, resulting in a fracture angle of $\theta \sim 0°$ rather than close to 45°. In this case, the new fracture criterion is reduced to the maximum normal stress criterion.

The reason for the small value of σ_f may be linked to the formation of pre-cracks in the particles already during the extrusion process, as indicated by arrows in Fig. 10 for the as-extruded sample with 60 vol.% glass reinforcement. In addition, owing to the milling procedure, the surface of the glassy particles is rough and irregular and, consequently, the stress distribution within the particles is complex and inhomogeneous under the applied load. As a result, this will reduce σ_f and make the particle prone to fracture along the compression direction.

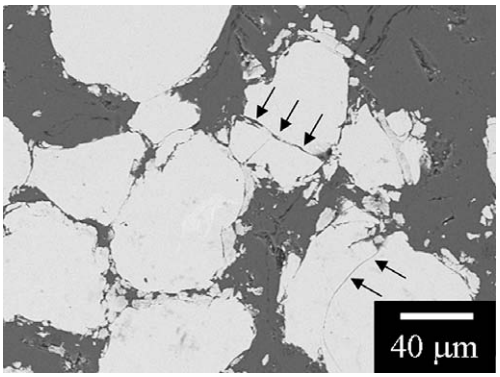

Fig. 10. SEM micrograph for the as-extruded composite 60 vol.% ($f = 60$) glass reinforcement, revealing the formation of pre-cracks.

4. Conclusions

Al-based metal matrix composites with high strength combined with considerable plastic deformation were synthesized using P/M methods by consolidation of elemental Al powder blended with different amounts of metallic glass reinforcements. The glass reinforcement was produced by MA of elemental powder mixtures with composition $Zr_{57}Ti_8Nb_{2.5}Cu_{13.9}Ni_{11.1}Al_{7.5}$. In order to take advantage of the viscous flow behavior of the glassy powder, the MMC with different amounts of glass reinforcements were consolidated into highly dense bulk specimens by hot pressing followed by hot extrusion at temperatures within the SCL region. Room temperature compression tests reveal that the addition of the glass reinforcement is very effective for improving the mechanical properties compared with pure Al. The compressive strength increases from 155 MPa for pure Al to 200 MPa for the composite with 40 vol.% glass reinforcement while retaining a fracture strain of ~70%. With the volume fraction of the glassy phase increasing to 60 vol.%, the compressive strength further increases to ~250 MPa, and the fracture strain is reduced to ~40%. SCEMA-based methods were used to model the elastoplastic deformation of the consolidated specimens. The yield strength used in the calculations was obtained by dislocation strengthening and optimized using the shear lag model in order to account for the effect of particle contiguity. The calculations are in good agreement with the experimental results when particle cracking during deformation is considered, indicating that the SCEMA method is applicable for modeling the deformation behavior of MMC containing large volume fractions of reinforcing particles. Finally, a suitable fracture criterion was used to explain the unusual distensile failure mode observed in the reinforcing glassy particles on the base of the critical particle fracture stress calibrated from SCEMA calculations.

Acknowledgments

The authors thank M. Frey, H.-J. Klauß and H. Schulze for technical assistance, and M. Stoica and S. Venkataraman for stimulating discussions. This work was supported by the German Science Foundation under grant Ec 111/16-2. G. Liu acknowledges the Alexander von Humboldt Foundation for financial support. K.G. Prashanth is grateful for the financial support provided by the "DAAD–IIT Masters Sandwich Program" for his stay at IFW Dresden.

References

[1] Clyne TW, Withers PJ. An introduction to metal matrix composites. Cambridge: Cambridge University Press; 1993.
[2] Kainer KU. Metal matrix composites. Custom-made materials for automotive and aerospace engineering. Weinheim: Wiley-VCH; 2006.
[3] Murakami Y. In: Cahn RW, Haasen P, Kramer EJ, editors. Materials science and technology, vol. 8. New York: VCH; 1996. p. 213.
[4] Miracle DB. Comp Sci Tech 2005;65:2526.
[5] Embury JD, Lloyd DJ, Ramachandran TR. In: Vasudevan AK, Doherty RD, editors. Aluminum alloys – contemporary research and applications, vol. 31. New York: Academic Press; 1989. p. 579.
[6] Guo X, Derby B. Prog Mater Sci 1995;39:411.
[7] Harrigan Jr WC. Mater Sci Eng A 1998;244:75.
[8] Slipenyuk A, Kuprin V, Milman Y, Goncharuk V, Eckert J. Acta Mater 2006;54:157.
[9] Tan MJ, Zhang X. Mater Sci Eng A 1998;244:80.
[10] Yu P, Kim KB, Das J, Baier F, Xu W, Eckert J. Scripta Mater 2006;54:1445.
[11] Lee MH, Kim JH, Park JS, Kim JC, Kim WT, Kim DH. Scripta Mater 2004;50:1367.
[12] Scudino S, Surreddi KB, Sager S, Sakaliyska M, Kim JS, Löser W, et al. J Mater Sci 2008;43:4518.
[13] Inoue A. Prog Mater Sci 1998;43:365.
[14] Johnson WL. MRS Bull 1999;24:42.
[15] Lin XH, Johnson WL. J Appl Phys 1995;78:6514.
[16] Das J, Tang MB, Kim KB, Theissmann R, Baier F, Wang WH, et al. Phys Rev Lett 2005;94:205501.
[17] Smagorinski ME, Tsantrizos PG, Grenier S, Cavasin A, Brzezinski T, Kim G. Mater Sci Eng A 1998;244:86–90.
[18] Erich DL. Prog Powder Metall 1986;46:45.
[19] ASTM E9-89aR00, Standard Test Methods for Compression Testing of Metallic Materials at Room Temperature. West Conshohocken, PA: ASTM; 2000.
[20] Scudino S, Eckert J, Yang XY, Sordelet DJ, Schultz L. Intermetallics 2007;15:571.
[21] Scudino S, Eckert J, Schultz L. J Mater Res 2004;19:2211.
[22] Eckert J. Mater Sci Eng A 1997;226:364.
[23] Busch R, Bakke E, Johnson WL. Acta Mater 1998;46:4725.
[24] Deledda S, Eckert J, Schultz L. Mater Sci Eng A 2004;375–377:804.
[25] Scudino S, Venkataraman S, Eckert J. J Alloys Comp 2008;460:263.
[26] ASTM E6-03, Standard Terminology Relating to Methods of Mechanical Testing, Annual Book of ASTM Standards, vol 03.01. West Conshohocken, PA: ASTM; 2003.
[27] Kim HS. Mater Sci Eng A 2000;289:30.
[28] Chawla KK. Composite materials: science and engineering. New York: Springer; 1987. p. 177.
[29] Kelly A. Particle and fibre reinforcement in strengthening methods in crystals. London: Applied Science; 1971. p. 433.
[30] Humphreys FJ. In: Anderson SI, Lilholt H, Pedersen OB, editors. Mechanical and physical behavior of metallic and ceramic composites. Denmark: Risø Nat Lab; 1988. p. 51.
[31] Miller WS, Humphreys FJ. Scripta Metall 1991;25:33.
[32] Hansen N. Acta Metall Mater 1977;25:863.
[33] Arsenault RJ, Wang L, Feng CR. Acta Metall Mater 1991;39:47.
[34] Arsenault RJ, Shi N. Mater Sci Eng 1986;81:175.
[35] Brown LM, Stobbs WM. Phil Mag 1976;34:351.

[36] Metals Handbook, 9th ed., vol. 2. Properties and selection: nonferrous alloys and pure metals. Materials Park, OH: American Society for Metals; 1979.
[37] Wang WH, Dong C, Shek CH. Mater Sci Eng R 2004;44:45.
[38] Miserez A, Mortensen A. Acta Mater 2004;52:5331.
[39] Starink MJ, Syngellakis S. Mater Sci Eng A 1999;270:270.
[40] Mattern N, Kühn U, Hermann H, Roth S, Vinzelberg H, Eckert J. Mater Sci Eng A 2004;375–377:351.
[41] Miserez A, Rossell A, Mortensen A. Acta Mater 2004;52:1337.
[42] Christensen RM, Lo KH. J Mech Phys Solids 1979;27:315.
[43] Kreher W, Pompe W. Internal stress in heterogeneous solids. Berlin: Akademie-Verlag Berlin; 1989. p. 91.
[44] Wilkinson DS, Wolfgang P, Oeschner M. Prog Mater Sci 2001;46:379.
[45] Wilkinson D, Maire E, Embury D. Mater Sci Eng A 1997;233:145.
[46] Nan CW, Clarke DR. Acta Mater 1996;44:3801.
[47] Nan CW, Yuan RZ. Phys Rev B 1993;48:3042.
[48] Nan CW. Physics of inhomogeneous inorganic materials. Beijing: Science Press; 2005. p. 192.
[49] Liu G, Sun J, Nan CW, Chen KH. Acta Mater 2005;53:3459.
[50] Weibull W. J Appl Mech-Trans ASTM 1951;18:293.
[51] Zhang ZF, He G, Eckert J, Schultz L. Phys Rev Lett 2003;91:045505.
[52] Zhang ZF, Eckert J, Schultz L. Acta Mater 2003;51:1167.
[53] Conner RD, Dandliker RB, Johnson WL. Acta Mater 1998;46:6089.
[54] Zhang ZF, He G, Eckert J. Phil Mag 2005;85:897.
[55] Zhang ZF, Eckert J. Phys Rev Lett 2005;94:094301.